Int. J. Electrochem. Sci., 15 **(2020)** 11709 – 11722, doi: 10.20964/2020.12.49

International Journal of
ELECTROCHEMICAL
SCIENCE
www.electrochemsci.org

SnO_2/TiO_2 Nanocomposite Prepared by Pulsed Laser Deposition as Anode Material for Flexible Quasi-solid-state Lithium-Ion Batteries

Wanli Wang[1], Yuhao Li[2], Liwei Li[1,], Licheng Wang[3], Kai Wang[1,*]*

[1] School of Electrical Engineering, Qingdao University, Qingdao, 266071, China
[2] Pingyi Power Supply Company of State Grid Shandong Electric Power Company, Linyi, 273316, China
[3] School of Information Engineering, Zhejiang University of Technology, Hangzhou, 310023, China
[*]E-mail: wkwj888@163.com, ytllw@qdu.edu.cn

Received: 23 August 2020 / *Accepted:* 14 October 2020 / *Published:* 31 October 2020

SnO_2/TiO_2 nanoparticle structure were prepared by alternately depositing SnO_2 and TiO_2 by pulsed laser deposition (PLD) system as the anode of lithium-ion batteries. The prepared SnO_2/TiO_2 electrode material has a high reversible capacity (809.30 mAh g^{-1} capacity after cyclic testing for 100 times at a current density of 100 mA g^{-1}) and a high rate capability (488.71 mAh g^{-1} capacity at a current density of 3000 mA g^{-1}). The nanoparticle membrane structure significantly shortens the diffusion distance of lithium ions and effectively buffers the stress generated in the process of cyclic charging and discharging. Moreover, the two oxide particles, SnO_2 and TiO_2, are distributed at intervals throughout the electrode, which greatly limits the position migration of nanoparticles in the circulation process, thereby it significantly enhances the integrity and stability of the electrode structure in the circulation process. Besides, the SnO_2/TiO_2 film with nanoparticle structure was successfully applied to the flexible quasi-solid-state batteries, which can easily light up the blue high-power LED in different bending states. These excellent electrochemical properties confirm the importance of our work for providing a new strategy to produce anode materials for lithium-ion batteries. Our work may shed light on the design of anode materials in high-performance lithium-ion batteries, exceptionally thin-film micro batteries and flexible lithium-ion batteries.

Keywords: nanoparticle structure; pulsed laser deposition; high reversible capacity; high rate capability; flexible quasi-solid-state batteries

1. INTRODUCTION

With the rapid continuous progress of science and technology, the demand for energy is increasing of human society [1-7]. Fossil fuels have gradually dried up and caused severe environmental

pollution [8-13]. Clean and efficient energy storage devices play a vital role in coping with global warming and energy crisis [14-21]. There are many ways of energy storage technology. [22-27]. Among them, as a new type of high-energy green battery, lithium-ion battery has attracted much attention and is known as "green power supply" due to its high energy efficiency, low self-discharge rate, high working voltage, long cycle life, high energy density, no toxic substances, and high current charging and discharging. In recent years, with the development of technology, the cost of lithium-ion batteries has been dramatically reduced, and it has become the mainstream choice for mobile equipment, electric vehicles, and energy storage power stations. Consumer electronics and electric vehicles require higher and higher battery life and charging speed [28-30]. Especially in the field of electric vehicles, consumers' desire to purchase electric vehicles is closely related to the price, charging speed and service life of electric vehicles. However, traditional electrode materials can no longer meet people's increasingly high-performance requirements for lithium-ion batteries [31-38]. Taking electric vehicles as an example, the traditional graphite anode has poor rate capabilities and low lithium intercalation potential, which makes it difficult to meet the requirements of electric vehicles for high power characteristics and safety performance [39-47]. Therefore, the development of anode materials with faster-charging speed and more extended cycle performance has become one of the current research hotspots.

TiO_2, as an intercalated metal oxide, has the advantages of safe reaction potential (> 1.5 V *vs*. Li/Li^+), low cost of inserting and removing lithium ions, small volume change (2-3%), environmental friendliness and excellent cycle performance, which has aroused great attention. However, the electronic conductivity of this material is low, and its theoretical specific capacity is low, only 175-330 mAh g^{-1} [48, 49]. Moreover, its poor electronic conductivity and rate performance limit its application in the field of power batteries [50, 51].

Among metal oxides, SnO_2 has attracted extensive attention as an anode material because of its high theoretical specific capacity (782 mAh g^{-1}) and low working voltage (0.6 V, *vs* Li/Li^+) [52, 53]. The reaction process of SnO_2 can be divided into two stages. In the first stage, SnO_2 reacts with lithium ions to generate elementary substances Sn and Li_2O. The reaction process generates SEI films and is accompanied by a large number of irreversible reactions. In the second reaction stage, Sn combines with lithium ions to form alloy compounds, and lithium-ion storage mainly occurs in this stage. However, the volume of SnO_2 changes as much as 200% during charging and discharging, which seriously affects the cycle life and performance [54, 55].

Interestingly, the characteristics of SnO_2 and TiO_2 anode materials are just complementary. Therefore, a growing number of researchers has been devoted to the development of various SnO_2/TiO_2 nanostructured composites [56], including spherical structures [57-59], nanotubes [60, 61], nanowires [62-64] and microcones [65]. Compared with tin dioxide and titanium dioxide anode materials alone, they all show better electrochemical performance. However, so far, there have been few reports on layered SnO_2 and TiO_2 nanocomposites. Fan et al. proposed to manufacture a self-supported amorphous SnO_2/TiO_2 nanocomposite film with good reversible capacity, but the energy density per unit area of the film is relatively low (175μA h cm^{-2}).

In this study, to further improve the energy density per unit area, SnO_2/TiO_2 nanocomposites with a thickness of 300 nm were obtained by alternately depositing tin dioxide (20nm) and titanium dioxide (5 nm) in PLD system for 12 cycles, and the energy density per unit area can reach 229μA h cm^{-}

[2]. This structure is formed by stacking multiple layers of ultrafine SnO_2 and TiO_2 particles, and the two oxide components are distributed in the whole electrode at intervals. The nanoparticle membrane structure can significantly reduce the diffusion distance of lithium ions and effectively buffer the stress released in the process of cyclic charging and discharging. Concurrently, the layered structure formed by the accumulation of nanoparticles dramatically increases the contact area between the particles and is beneficial to the reaction [66, 67]. More importantly, the two components are alternately arranged layer by layer, and one component is separated from the other, which dramatically limits the position migration of nanoparticles in the circulation process [68-70], thus significantly limiting the aggregation and growth of nanoparticles, and greatly improving the integrity and stability of the electrode structure in the circulation process. In addition, the prepared SnO_2/TiO_2 electrode material has an amorphous structure [71, 72], which can better play the role of buffering stress, and also limit the destruction of the electrode structure. Based on the above structural design, the prepared SnO_2/TiO_2 electrode material has a high reversible capacity (809.30 mAh g^{-1} capacity after cyclic testing for 100 times at a current density of 100 mA g^{-1}) and a high rate capability (488.71 mAh g^{-1} capacity at a current density of 3000 mA g^{-1}).

2. MATERIALS AND METHODS

2.1 Pulsed laser deposition

Pulsed laser deposition (PLD), also known as pulsed laser ablation (PLA), is a widely used thin-film deposition technology [73, 74]. Pulsed laser rapidly vaporizes the target to generate a thin film with the same composition as the target. The unique feature of PLD is that the energy source (pulsed laser) is located outside the vacuum chamber. In this way, during material synthesis, the dynamic range of working pressure is extensive, reaching 10–10 Torr ~ 100 Torr. By controlling the coating pressure and temperature, a series of nanostructures and nanoparticles with unique functions can be synthesized. Besides, PLD is a "digital" technology that performs process control (Å /pulse) on a nanometer scale. Also, PLD also has the advantages of fast growth speed, strong orientation, high film resolution, easy fabrication of multilayer films, and heterogeneous films.

2.2 Preparation of SnO_2/TiO_2 anode materials

Multilayer SnO_2/TiO_2 anode materials were prepared by PLD method: rutile titanium dioxide and stannic oxide were used as targets (purity 99.9%). The experimental parameters are as follows: the substrate pressure is 10pa, the oxygen pressure is 2 Pa, the laser wavelength is 248 nm, the pulse energy is 300 mJ, and the repetition frequency is 5 Hz. SnO_2 and TiO_2 are alternately deposited on a copper foil substrate, *i.e.*, a layer of SnO_2 is deposited on the substrate first, and then a layer of TiO_2 is deposited on the obtained SnO_2, the thickness of each layer of SnO_2 and TiO_2 is 20 nm and 5 nm respectively, and the SnO_2/TiO_2 anode material with a thickness of 300 nm and obtained by alternately depositing 12 cycles. In addition, as a comparison, we also prepared pure SnO_2 and TiO_2 anode materials respectively under the

same conditions. The whole reaction was carried out at room temperature. The deposition rate of SnO_2/TiO_2 anode material was determined by an atomic force microscope (AFM, Parker system XE7).

2.3 Synthesis of lithium-ion conducting gel polymerization electrolyte

First, P(VDF-HFP) was dissolved in a mixture of dimethylformamide (DMF) and deionized water (mass ratio of 15:85:3) at 80 ^oC. Subsequently, the prepared viscous solution was poured into the petri dish and immersed in a constant temperature 80 ^oC water bath to obtain a uniform white P(VDF-HFP) membrane. The prepared P(VDF-HFP) film was then dried for 12 hours under a vacuum condition of 100 ^oC, and then punched into a diaphragm with a diameter of 19 mm for use in the preparation of a half-cell. Finally, the cut P(VDF-HFP) membrane was immersed in an organic electrolyte (1 M $LiPF_6$ dissolved in a mixture of ethyl carbonate (EC) and dimethyl carbonate (DEC) by volume ratio of 1:1) for more than 48 hours to obtain a conductive gel polymer electrolyte.

2.4 Characterization of physical properties of materials

X-ray diffraction (XRD) analysis: The samples were tested by Rigaku-D/Max X-ray diffractometer of Rigaku Corporation, and the light source used was Cu Kα.

Field-emission scanning electron microscopy (FESEM) analysis: JSM-6700F field emission scanning electron microscope produced by JEOL was used to characterize the surface morphology.

2.5 Electrochemical measurement

Preparation of electrode sheet and assembly of battery: Celgard 2250 membrane is used as the diaphragm; ethyl carbonate (EC)/ dimethyl ethyl carbonate (DEC)/ $LiPF_6$ (volume ratio 1: 1: 1) (KeJing Group) is used as a standard electrolyte; and lithium metal sheet is used as counter electrode and a reference electrode in this experiment. The whole battery assembly process was carried out in an argon glove box. The model of the battery used in the experiment was the CR-2032 button battery (KeJing Group).

Electrochemical performance test: in this experiment, the Land-ct2001A battery test system is used to carry out charging and discharging tests at different current rates; the charging and discharging voltage range of the half-cell is 0.01 V–3.0 V. The cyclic voltammetry curve and electrochemical impedance spectroscopy (EIS) were tested by CHI660E electrochemical workstation; the potential range was 0.01 - 3.0 V, the scanning rate was 0.2 mV s^{-1}, and the frequency ranges was 0.01 – 10^5 Hz with a voltage amplitude of 5 mV. The weight of the SnO_2/TiO_2 film was measured by a METTLER TOLEDO analytical balance with an accuracy of 0.005 mg.

3. RESULTS AND DISCUSSION

Fig. 1 shows the preparation process of SnO_2/TiO_2 film with nanoparticle structure. With PLD technology, the stannic oxide and rutile titanium dioxide deposit on the copper foil substrate and thus form SnO_2/TiO_2 thin films. (Specific preparation details can be found in the experimental part).

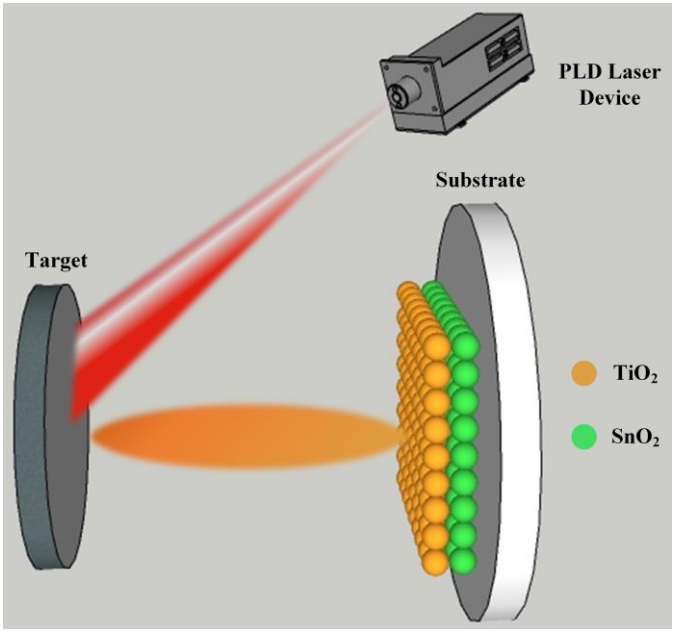

Figure 1. Schematic diagram of SnO_2/TiO_2 film with nanoparticle structure prepared by PLD technology (The experimental parameters are as follows: the substrate pressure is 10pa, the oxygen pressure is 2 Pa, the laser wavelength is 248 nm, the pulse energy is 300 mJ, and the repetition frequency is 5 Hz.).

Firstly, pure SnO_2, pure TiO_2 and SnO_2/TiO_2 were characterized by XRD. The crystal structure of the prepared materials can be studied by XRD. As shown in Fig. 2, except the Cu peak shown on the copper foil substrate, no other diffraction peaks were observed in the XRD patterns of the three samples. Besides, no obvious grains were found from the TEM analysis diagram in Fig. 3, and the electron diffraction was amorphous. This indicates that pure tin oxide, pure titanium oxide and layered SnO_2/TiO_2 prepared by PLD are amorphous, which may be related to low deposition temperature.

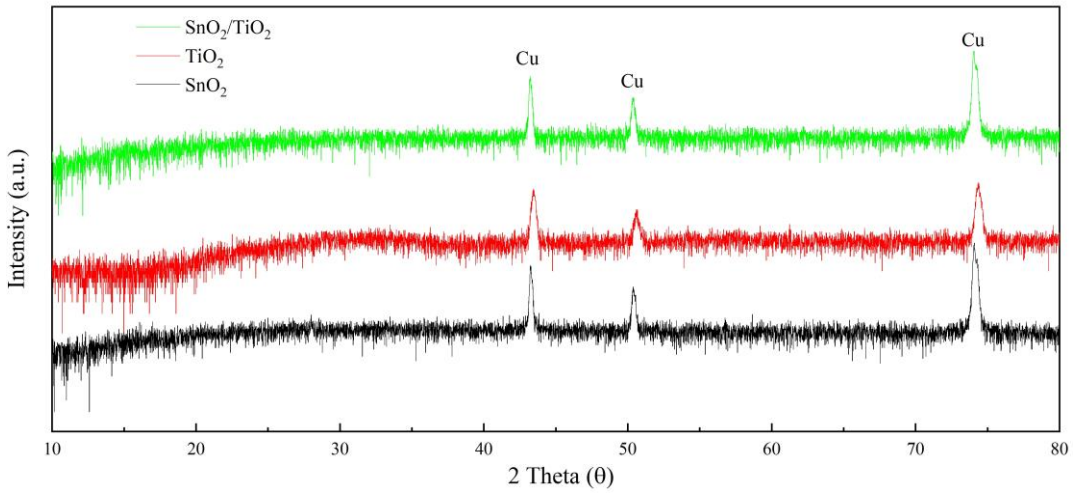

Figure 2. XRD patterns of pure SnO_2, pure TiO_2 and SnO2/TiO2 electrode materials. (The samples were tested by Rigaku-D/Max X-ray diffractometer of Rigaku Corporation, and the light source used was Cu Kα.)

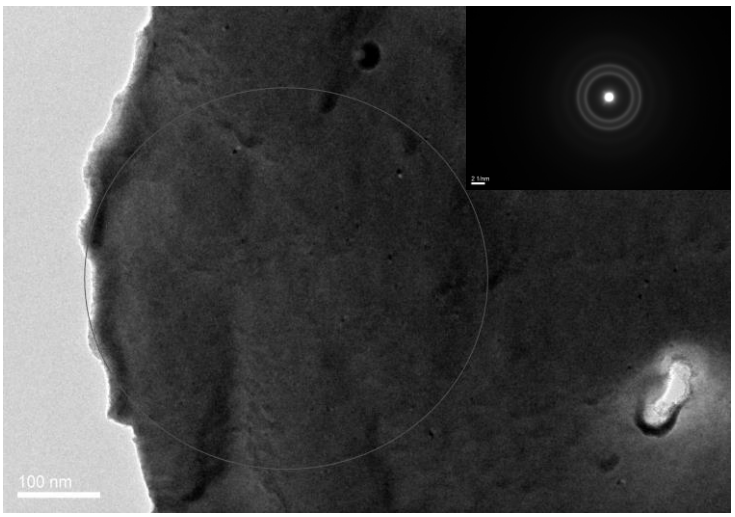

Figure 3. The TEM image of SnO_2/TiO_2 (the inset is the SAED pattern of SnO_2/TiO_2).

Next, we tested the electrochemical performance of the prepared SnO_2/TiO_2. Cyclic voltammetry curves can be used to study the electrode reaction process in a specific potential range and further study its reaction mechanism. Therefore, the SnO_2/TiO_2 electrode material was first characterized by cyclic voltammetry, and the scanning voltage range was 0.01-3.0 V. Fig. 4 shows the CV curve for the first five cycles of SnO_2/TiO_2 obtained at a scanning rate of 0.2 mV s^{-1}. Five reduction peaks were observed during the first charge-discharge process. The first small reduction peak at approximately 1.72 V corresponds to the formation of Li_xTiO_2 and reacts: x Li^+ + x e^- + $TiO_2 \rightarrow Li_xTiO_2$ [75, 76]. The second peak at approximately 1.22 V did not appear in the following four cycles, indicating that the reaction may be closely related to the formation of SEI film. The third strong peak centered at 0.93 V corresponds to the formation of SEI interface and the reduction of tin dioxide to Sn and the formation of Li_2O: 4 Li^+ + 4 e^- + $SnO_2 \rightarrow$2 Li_2O + Sn [77, 78]. The remaining two peaks at low potentials of 0.45 V and 0.22 V can be attributed to the alloying process of Li-Sn: 4.4 Li^+ + 4.4 e^- + $Sn \rightarrow Li_{4.4}Sn$ [69, 79]. There are three obvious oxidation peaks during the charging process. The oxidation peak at 0.50 V can correspond to the dealloying process of Li_xSn to Sn, while the oxidation peak at 1.25 V can be attributed to the reversible conversion of Sn to SnO_2. The oxidation peak at 1.87 V can be attributed to the lithium removal reaction of TiO_2. As the cycle continues, the volt-ampere curves of the following four cycles coincide indicating that the SnO_2/TiO_2 electrode has good reversibility of lithium-ion storage.

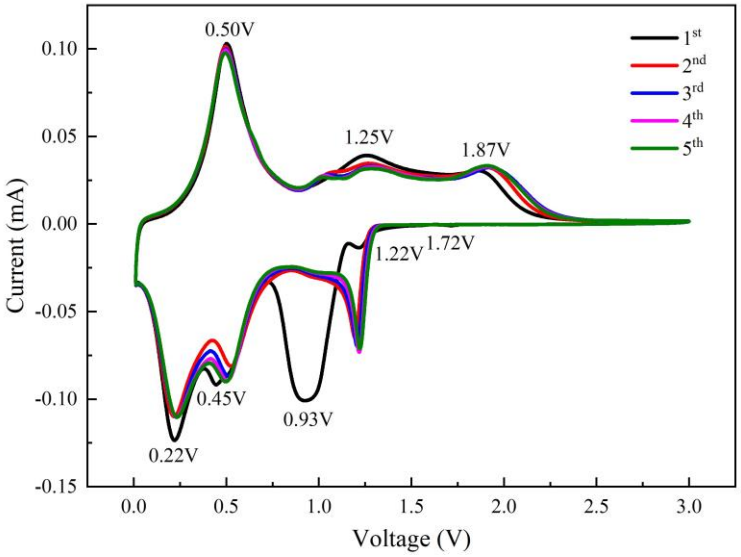

Figure 4. Cyclic voltammogram of SnO_2/TiO_2 electrode material at a scanning rate of 0.2 mV s^{-1}. (Cyclic voltammetry (CV) measurements were obtained by a CHI660E electrochemical workstation, the potential range was 0.01 V–3.0 V)

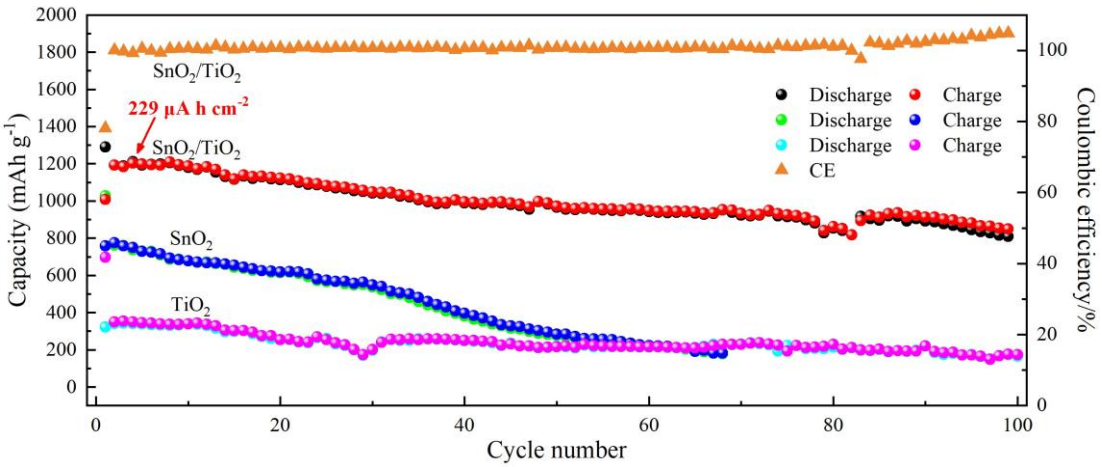

Figure 5. Cyclic performance of pure SnO_2, pure TiO_2 and SnO_2/TiO_2 electrode materials at 100 mA g^{-1}. (Cyclic voltammetry (CV) measurements were obtained by a CHI660E electrochemical workstation)

The SnO_2/TiO_2 electrode materials showed significant improvement in the cycling performance of the battery in electrochemical tests. Fig. 5 shows the cycling performance of the three electrode materials. As can be seen from the figure, during the cycle, the capacity of SnO_2 decreases rapidly with the increase of cycle times. After only 70 cycles, the specific capacity of SnO_2 decreases from 762.2 mAh g^{-1} to 178.0 mAh g^{-1}, which is only 23.4% of the specific capacity of the second discharge. The capacity of TiO_2 decreases slightly as the cycle progresses, but due to its low initial specific capacity, only 165.8 mAh g^{-1} remains after 100 cycles. In contrast, SnO_2/TiO_2 shows better cycle stability and higher specific capacity, and after 100 cycles of testing, the specific discharge capacity is still as high as

809.3 mAh g^{-1}. Besides, the initial specific discharge and charge capacities of SnO_2/TiO_2 are 1290.6 mAh g^{-1} and 1007.9 mAh g^{-1}, respectively, corresponding to a coulombic efficiency (CE) as high as 78.1%, which is higher than the previously reported results of most SnO_2–TiO_2 anode electrodes (Table 1). And Table 2 lists the relevant parameters of SnO_2/TiO_2 SnO_2 and TiO_2 three lithium-ion batteries anode materials used in this paper for the convenience of performance comparison.

Table 1. Comparison of electrochemical properties between SnO_2/TiO_2 electrode materials prepared and SnO_2–TiO_2-based lithium-ion batteries anode materials published earlier by other researchers.

Anode materials	Initial coulombic efficiency	Ref.
SnO_2/TiO_2 nanoparticle	78.1%	This work
SnO_2/TiO_2 films	75.9%	[56]
SnO_2/TiO_2 nanocomposites	64.2%	[59]
3D nano-network TiO_2@SnO_2 film	62.9%	[63]
TiO_2@SnO_2@TiO_2 triple-shell nanotube	52.8%	[60]
SnO_2/TiO_2 multishell microspheres	46.8%	[58]
TiO_2@SnO_2@TiO_2 hollow spheres	43.8%	[79]

Table 2. Comparison of parameters of SnO_2/TiO_2, SnO_2 and TiO_2 lithium ion anode materials.

Anode materials	Specific capacity of the second cycle	Initial coulombic efficiency	Specific capacity after 70 cycles	Coulombic efficiency after 70 cycles
SnO_2/TiO_2	1192 mAh g^{-1}	78.1%	923.5 mAh g^{-1}	77.5%
SnO_2	762.2 mAh g^{-1}	73.9%	178.0 mAh g^{-1}	23.4%
TiO_2	340.5 mAh g^{-1}	216.7%	233.0 mAh g^{-1}	68.4%

The improvement of cycle stability is due to the design of SnO_2/TiO_2 nanoparticle membrane structure, which better ensures the structural integrity of electrode materials. Figure 6 shows the morphological changes of SnO_2 and SnO_2/TiO_2 after 200 cycles of testing. The surface of the SnO_2 electrode material in Fig. 6(a) shows a large number of cracks, while SnO_2/TiO_2 electrode material in Fig. 6(b) shows a good morphology without obvious cracks or a large amount of agglomeration, which may be due to the reasonable structural design of SnO_2/TiO_2 electrode material. Small particles enable electrode materials to withstand stress better, and dense accumulation of particles significantly inhibits migration and aggregation of active substance particles. In addition, the layered structure makes the volume expansion change of SnO_2 limited by the TiO_2 layer, making the electrode material show a smaller volume change in the cyclic reaction process, and dramatically ensuring the structural integrity of the electrode material.

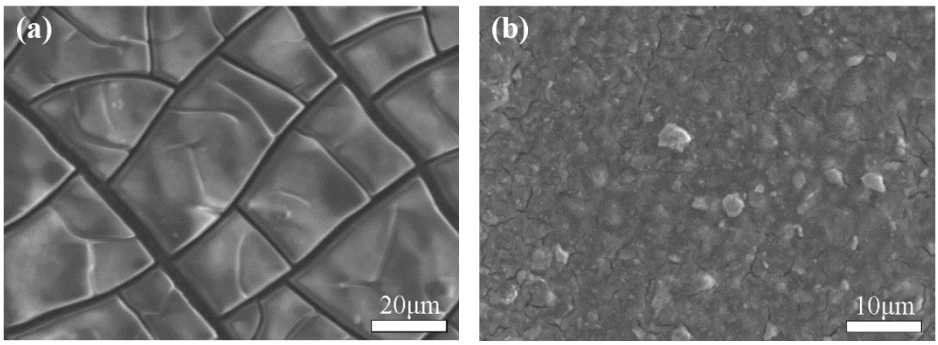

Figure 6. SEM images of pure SnO_2 and SnO_2/TiO_2 electrode materials after 200 cycles of testing (SM-6700F field emission scanning electron microscope produced by JEOL was used to characterize the surface morphology.), (a) pure SnO_2; (b) SnO_2/TiO_2 electrode materials.

Besides better cycle stability and higher specific capacity, SnO_2/TiO_2 electrode materials also show excellent rate capability. Fig. 7 presents a rate capability test curve of SnO_2/TiO_2 electrode under different current densities in the range of 500 mAh g^{-1}-3000 mAh g^{-1}. At current densities of 500, 1000, 1500, 2000 and 3000 mAh g^{-1}, each current density test cycle was 10 times, and then the current density was restored to 500mAh g^{-1} for 10 times. As can be seen from the figure, the average discharge specific capacity of the electrodes is 898.59, 760.44, 694.8, 563.67 and 488.71 mAh g^{-1} respectively, when the current density is 500, 1000, 1500, 2000 and 3000 mAh g^{-1} respectively. When the current density returns to 500 mAh g^{-1}, the specific discharge capacity returns to 742.87 mAh g^{-1} and the capacity retention rate is 82.67%. The SnO_2/TiO_2 electrode has an excellent rate capability, which may be attributed to the unique structure of the SnO_2/TiO_2 electrode material. Firstly, as an amorphous material, SnO_2/TiO_2 electrode material can promote the rapid diffusion of lithium ions through defects in amorphous phase, thus possessing high lithium-ion conductivity. Secondly, the compact SnO_2/TiO_2 electrode material greatly shortens the diffusion distance of lithium ions, which is more conducive to the rapid intercalation and deintercalation of lithium ions and provides capacitive lithium storage.

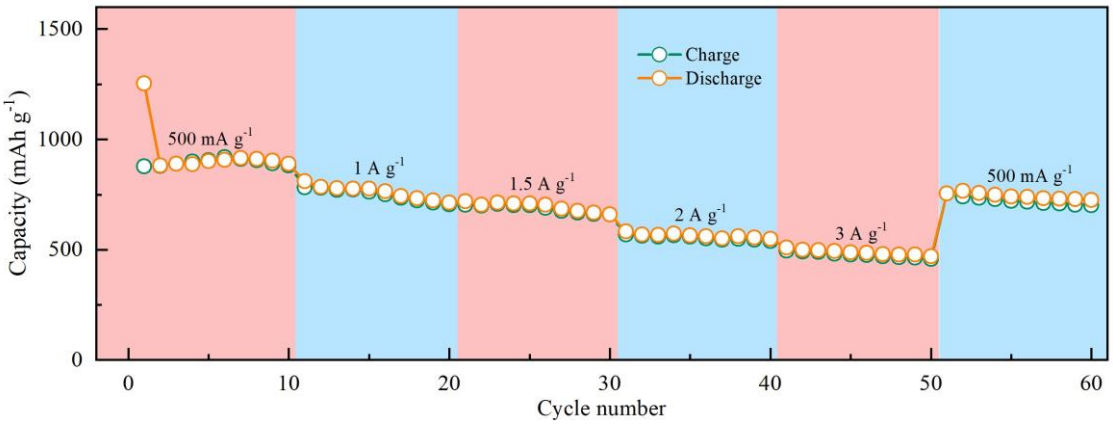

Figure 7. Rate capabilities of SnO_2/TiO_2 electrode material from 500 to 3000 mA g^{-1} (the Land-ct2001A battery test system is used to carry out charging and discharging tests at different current rates).

The improvement of the electrochemical performance of SnO_2/TiO_2 electrode materials was further confirmed by EIS measurements. As shown in Fig. 8, each curve consists of two parts: a concave semicircle in the high-frequency region and a slope line in the low-frequency region. The semicircle part is due to the charge transfer process, while the diagonal part is due to the diffusion process of lithium ions in the active material. According to the three curves, it is easy to know that the impedance of SnO_2/TiO_2 electrode material is much smaller than that of pure SnO_2, indicating that the conductivity is improved after the combination of SnO_2 and TiO_2. The lithium-ion diffusion rate of SnO_2/TiO_2 electrode material is much faster than TiO_2, indicating that the lithium-ion diffusion behavior is also enhanced. This result also well explains the excellent rate capability and cycle stability of SnO_2/TiO_2 electrode materials.

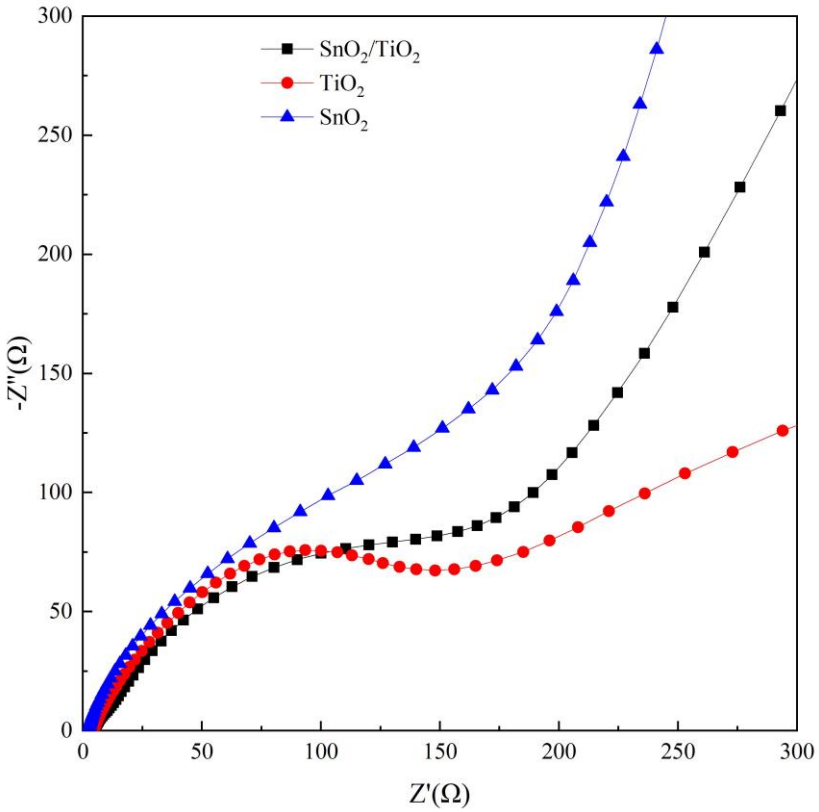

Figure 8. EIS diagram of pure SnO_2, pure TiO_2 and SnO_2/TiO_2 electrode materials (electrochemical impedance spectroscopy (EIS) were tested by CHI660E electrochemical workstation).

As a self-supporting electrode material, SnO_2/TiO_2 films with nanoparticle structure can be widely used in solid film batteries, lithium-ion batteries, supercapacitors, lithium-air batteries, electrocatalytic hydrogen evolution and many other fields. In this paper, using P(VDF-HFP) film as Li^+ conductive gel polymer electrolyte, SnO_2/TiO_2 film was successfully applied to flexible quasi-solid-state batteries. As shown in Figure 9, the assembled flexible half-cell can light up the high-power blue LED in different bending states (or even completely rolled into a roll), which sufficiently proves its excellent application in flexible solid-state batteries.

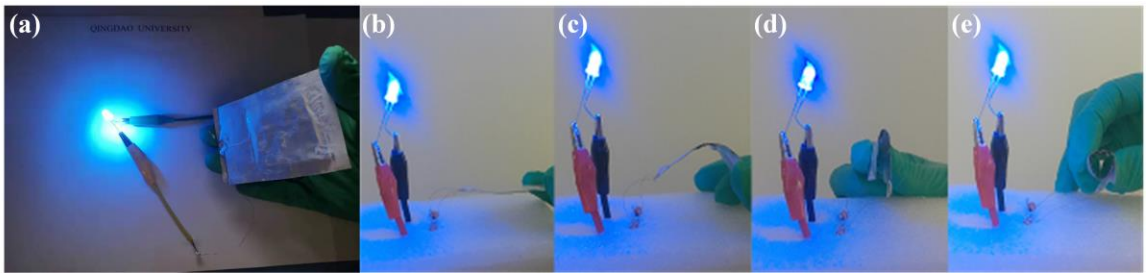

Figure 9. Application of SnO_2/TiO_2 film to a flexible quasi-solid-state battery. (a) Photo of the soft-packaged half-cell, (b-e) The flexible half-cell illuminates the blue LED under different bending conditions.

4. CONCLUSIONS

SnO_2/TiO_2 anode materials with nanoparticle structure were prepared by alternately depositing SnO_2 and TiO_2 through the PLD system. Due to the complementary characteristics of SnO_2 and TiO_2 and the intelligent nanoparticle structure design, the prepared SnO_2/TiO_2 anode material accelerates not only the diffusion of lithium ions, but also better limits the change of the electrode structure in the reaction process, thus significantly improving the integrity and stability of the electrode structure in the circulation process. Thus, it shows high reversible capacity (809.30 mAh g^{-1} capacity after 100 cycles at a current density of 100 mA g^{-1}) and high rate capability (488.71 mAh g^{-1} capacity at a current density of 3000 mA g^{-1}). The preservation of structure and excellent electrochemical performance during the cyclic reaction show that this work provides a new idea for the production of anode electrode materials of SnO_2/TiO_2 lithium ion batteries, and has a very considerable application prospect in high-performance lithium-ion batteries, especially thin-film micro-batteries and flexible lithium-ion batteries.

ACKNOWLEDGEMENTS
This research was supported by the Shandong Science and Technology Development Plan (No. 2019GGX104019), the Project of Shandong Province Higher Educational Science and Technology Program (J18KA316), the Liaoning Science and Technology Plan (No. 20180550573), and Guangdong Basic and Applied Basic Research Foundation (2019A1515110706).

CONFLICTS OF INTEREST
The authors declare no conflict of interest.

References

1. J.M. Tarascon, M. Armand, *Nature*, 414 (2001) 359.
2. M.D. Tikekar, S. Choudhury, Z. Tu and L.A. Archer, *Nat. Energy*, 1 (2016) 16114.
3. D.L. Yuan, M.T. Sun, M.Z. Zhao, S.F. Tang, J.B. Qi, X.Y. Zhang, K. Wang, B. Li. *Int. J. Electrochem. Sci.*, 15 (2020) 8761.
4. M.R. Palacin, A. De Guibert, *Science*, 351 (2016) 1253292.
5. G.T. Xia, C. Li, K. Wang and L.W. Li, *Sci. Adv. Mater.*, 11 (2019) 1079.
6. Y.T. Zhou, Y.N. Huang, J.B. Pang and K. Wang, *J. Power Sources*, 440 (2019) 227149.

7. Y.T. Zhou, Y.N. Wang, K. Wang, L. Kang, F. Peng, L.C. Wang and J.B. Pang, *Appl. Energy*, 260 (2020) 114169.
8. M. Arshad, H. Du, M.S. Javed, A. Maqsood, I. Ashraf, S. Hussain, W. Ma and H. Ran, *Ceram. Int.*, 46 (2020) 2238.
9. Q. Li, H.S. Li, Q.T. Xia, Z.Q. Hu, Y. Zhu, S.S. Yan, C. Ge, Q.H. Zhang, X.X. Wang and X.T Shang, *Nat. Mater.*, (2020) DOI: 10.1038/s41563-020-0756-y.
10. C. Duan, Y. Yu, J. Xiao, X. Zhang, L. Li, P. Yang, J. Wu and H. Xi, *Sci. China-Mater.*, 63 (2020) 667.
11. S.F. Tang, Z.T. Wang, D. Yuan, C. Zhang, Y.D. Rao, Z.B. Wang and K. Yin, *J. Clean Prod.*, 268 (2020) 122253.
12. S.F. Tang, J.C. Tang, D.L. Yuan, Z.T. Wang, Y.T. Zhang and Y.D. Rao, *RSC Adv.*, 10 (2020) 17627.
13. K. Wang, W.L. Wang, L.C. Wang, L.W. Li, *Energies*, 13 (2020) 5297.
14. H. Li, W. Chai and G. Henkelman, *J. Mater. Chem.*, 7 (2019) 23868.
15. H. Li, K. Shin and G. Henkelman, *J. Chem. Phys.*, 149 (2018) 174705.
16. H. Li, S. Guo, K. Shin, M.S. Wong and G. Henkelman, *ACS Catal.*, 9 (2019) 7957.
17. Q. Cheng, J. Pang, D. Sun, J. Wang, S. Zhang, F. Liu, Y. Chen, R. Yang, N. Liang and X. Lu, *InfoMat*, 2 (2020) 656.
18. X.X. Wang, W.Z. Song, M.H. You, J. Zhang, M. Yu, Z. Fan, S. Ramakrishna and Y.Z. Long, *ACS Nano*, 12 (2018) 8588.
19. C.Y. Bu, F.J. Li, K. Yin, J.B. Pang, L.C. Wang and K. Wang, *ACS Appl. Electron. Mater.*, 2 (2020) 863.
20. G.T. Xia, Y.N. Huang, F.J. Li, L.C. Wang, J.B. Pang, L.W. Li and K. Wang, *Front. Chem. Sci. Eng.*, (2020) DOI: 10.1007/s11705-11019-11901-11705.
21. X. Feng, Y. Zhang, L. Kang, L.C. Wang, C.X. Duan, K. Yin, J.B. Pang and K. Wang, *Front. Chem. Sci. Eng.*, (2020) DOI: 10.1007/s11705-11020-11956-11703.
22. F.L. Zhang, X.L. Teng, W.K. Shi, Y.F. Song, J. Zhang, X. Wang, H.S. Li, Q. Li, S.D. Li and H. Hu, *Appl. Surf. Sci.*, (2020) 146910.
23. X. Luo, F. Zhang, Q. Li, Q. Xia, Z. Li, X. Li, W. Ye, S. Li and C. Ge, *J. Phys.-Condes. Matter*, 32 (2020) 334001.
24. L.C. Wang, R. Yan, F. Bai, T.K. Saha and K. Wang, *IEEE Trans. Sustain. Energy*, 11 (2020) 2687.
25. Q. Xue, Y. Yang, Z. Gao, F. Liu, Q. Li, S. Li and G.X. Miao, *Appl. Phys. Lett.*, 109 (2016) 192407.
26. K. Wang, L. Li, Y. Lan, P. Dong and G.T. Xia, *Math. Probl. Eng.*, 2019 (2019) 2614327.
27. K. Wang, L.W. Li, T.Z. Zhang and Z.F. Liu, *Energy*, 70 (2014) 612.
28. M. Zhang, K. Wang and Y.T. Zhou, *Complexity*, 2020 (2020) 8231243.
29. S.F. Tang, Z.T. Wang, D. Yuan, Y. Zhang, J. Qi, Y. Rao, G. Lu, B. Li, K. Wang and K. Yin, *Int. J. Electrochem. Sci.*, 15 (2020) 2470.
30. J.R. Wu, K. Yin, M. Li, S. Xiao, Z.P. Wu, K. Wang, J.A. Duan and J. He, *Colloid Surf. A-Physicochem. Eng. Asp.*, 601 (2020) 125030.
31. K. Wang, C. Li and B.C. Ji, *J. Mater. Eng. Perform.*, 23 (2014) 588.
32. S.F. Tang, M.Z. Zhao, D.L. Yuan, X. Li, X.Y. Zhang, Z.B. Wang, T.F. Jiao, K. Wang, *Sep. Purif. Technol.*, 255 (2021) 117690.
33. K. Wang, S.Z. Zhou, Y.T. Zhou, J. Ren, L.W. Li and Y. Lan, *Int. J. Electrochem. Sci.*, 13 (2018) 10766.
34. K. Wang, L.W. Li, W. Xue, S.Z. Zhou, Y. Lan, H. Zhang and Z.Q. Sui, *Int. J. Electrochem. Sci.*, 12 (2017) 8306.
35. Y. Qin, Q. Li, J. Xu, X. Wang, G. Zhao, C. Liu, X. Yan, Y. Long, S. Yan and S. Li, *Electrochim. Acta*, 224 (2017) 90.
36. Q. Sun, X. Luo, Q. Xia, Y. Guo, J. Zhu, Q. Li and G. Miao, *J. Magn. Magn. Mater.*, 499 (2019) 166317.
37. J. Janek, W.G. Zeier, *Nat. Energy*, 1 (2016) 16141.

38. K. Wang, J.B. Pang, L.W. Li, S.Z. Zhou, Y.H. Li and T.Z. Zhang, *Front. Chem. Sci. Eng.*, 12 (2018) 376.
39. J. Hassoun, B. Scrosati, *J. Electrochem. Soc.*, 162 (2015) A2582.
40. Y. Mao, G. Li, Y. Guo, Z. Li, C. Liang, X. Peng and Z. Lin, *Nat. Commun.*, 8 (2017) 14628.
41. K. Wang, C.L. Liu, L.C. Wang, J.Y. Song, C.X. Duan, L.W. Li, *Complexity*, 2020 (2021) 1.
42. H. Shang, Z. Zuo, L. Li, F. Wang, H. Liu, Y. Li and Y. Li, *Angew. Chem.-Int. Edit.*, 57 (2018) 774.
43. X.L. Teng, F.L. Zhang, Q. Li, X. Wang, W.N. Ye, H.S. Li, J. Xu, D.R. Cao, S.D. Li and H. Hu, *J. Electrochem. Soc.*, (2020) DOI: 10.1149/1945-7111/abac1186.
44. X. Luo, F.L. Zhang, Q. Li, Q.T. Xia, Z.H. Li, X.K. Li, W.N. Ye, S.D. Li and C. Ge, *J. Phys.-Condes. Matter*, 32 (2020) 334001.
45. L. Guan, H. Hu, L.Q. Li, Y.Y. Pan, Y.F. Zhu, Q. Li, H.L. Guo, K. Wang, Y.C. Huang, M.D. Zhang, Y.C. Yan, Z.T. Li, X.L. Teng, J.W. Yang, J.Z. Xiao, Y.L. Zhang, X.S. Wang and M.B. Wu, *ACS Nano*, 14 (2020) 6222.
46. K. Wang, X. Feng, J.B. Pang, J. Ren, C.X. Duan and L.W. Li, *Int. J. Electrochem. Sci.*, 15 (2020) 9499.
47. K. Wang, L.W. Li and X.Z. Wu, *Int. J. Electrochem. Sci.*, 8 (2013) 6763.
48. X.L. Cheng, M. Hu, R. Huang and J.S. Jiang, *ACS Appl. Mater. Interfaces*, 6 (2014) 19176.
49. H. Hu, Q. Li, L.Q. Li, X.L. Teng, Z.X. Feng, Y.L. Zhang, M.B. Wu and J.S. Qiu, *Matter*, 3 (2020) 95.
50. L. Wang, T. Sasaki, *Chem. Rev.*, 114 (2014) 9455.
51. M. Zhi, W. Huang, Q. Shi, X. Jia, J. Zhang and S. Zheng, *J. Electrochem. Soc.*, 165 (2018) H804.
52. Q. Liu, Y. Dou, B. Ruan, Z. Sun, S.L. Chou and S.X. Dou, *Chem.-Eur. J.*, 22 (2016) 5853.
53. L. Li, B. Guan, L. Zhang, Z. Su, H. Xie and C. Wang, *J. Mater. Chem. A*, 3 (2015) 22021.
54. J. Zhang, H. Ren, J. Wang, J. Qi, R. Yu, D. Wang and Y. Liu, *J. Mater. Chem. A*, 4 (2016) 17673.
55. C. Hou, X.M. Shi, C.X. Zhao, X.Y. Lang, L.L. Zhao, Z. Wen, Y.F. Zhu, M. Zhao, J.C. Li and Q. Jiang, *J. Mater. Chem. A*, 2 (2014) 15519.
56. S. Fan, J. Zhang, X. Teng, X. Wang, H. Li, Q. li, J. Xu, D. Cao, S. Li and H. Hu, *J. Electrochem. Soc.*, 166 (2019) A3072.
57. R. Li, W. Xiao, C. Miao, R. Fang, Z. Wang and M. Zhang, *Ceram. Int.*, 45 (2019) 13530.
58. J.H. Jiang, S.N. Liu, Y.Y. Wang, Y. Liu, J. Fan, X.D. Lou, X.B. Wang, H. Zhang and L. Yang, *Chem. Eng. J.*, 359 (2019) 746.
59. X. Shi, S. Liu, B. Tang, X. Lin, A. Li, X. Chen, J. Zhou, Z. Ma and H. Song, *Chem. Eng. J.*, 330 (2017) 453.
60. J.H. Jean, H. Kwak, W.S. Kim, H.-C. Kim, K.Y. Park, H. Kim, H.S. Yang, W.R. Yu, K. Kang and S.H. Hong, *J. Solid State Electrochem.*, 21 (2017) 2365.
61. J.H. Jeun, K.Y. Park, D.H. Kim, W.S. Kim, H.C. Kim, B.S. Lee, H. Kim, W.R. Yu, K. Kang and S.H. Hong, *Nanoscale*, 5 (2013) 8480.
62. D.A. Zhang, Q. Wang, Q. Wang, J. Sun, L.L. Xing and X.Y. Xue, *Mater. Lett.*, 128 (2014) 295.
63. X. Li, Z. Zhu, G.P. Nayaka, J. Duan, D. Wang, P. Dong, L. Huang, J. Zhao, S. Sun and X. Yu, *J. Alloy. Compd.*, 752 (2018) 68.
64. Z. Yang, Q. Meng, Z. Guo, X. Yu, T. Guo and R. Zeng, *J. Mater. Chem. A*, 1 (2013) 10395.
65. H. Yoo, G. Lee and J. Choi, *RSC Adv.*, 9 (2019) 6589.
66. Y. Li, S. Yu, T. Yuan, M. Yan and Y. Jiang, *J. Power Sources*, 282 (2015) 1.
67. Y. Jiang, Y. Li, M. Yan and N. Bahlawane, *J. Mater. Chem.*, 22 (2012) 16060.
68. C. Guan, X. Wang, Q. Zhang, Z. Fan, H. Zhang and H.J. Fan, *Nano Lett.*, 14 (2014) 4852.
69. X. Li, X. Zhang, R. Wang, Z. Su, J. Sha and P. Liu, *J. Power Sources*, 336 (2016) 298.
70. Z. Yi, Q. Han, P. Zan, Y. Cheng, Y. Wu and L. Wang, *J. Mater. Chem. A*, 4 (2016) 12850.
71. R. Hu, W. Sun, H. Liu, M. Zeng and M. Zhu, *Nanoscale*, 5 (2013) 11971.
72. H. Liu, R. Hu, W. Sun, M. Zeng, J. Liu, L. Yang and M. Zhu, *J. Power Sources*, 242 (2013) 114.
73. E. Mohseni, E. Zalnezhad and A.R. Bushroa, *Int. J. Adhes. Adhes.*, 48 (2014) 238.

74. Q.H. Bao, C.Z. Chen, D.G. Wang, Q.M. Ji and T.Q. Lei, *Appl. Surf. Sci.*, 252 (2005) 1538.
75. H. Wang, Y. Yan and G. Chen, *J. Alloy. Compd.*, 778 (2019) 375.
76. O. Rhee, G. Lee and J. Choi, *ACS Appl. Mater. Interfaces*, 8 (2016) 14558.
77. S.Y. Lee, K.Y. Park, W.S. Kim, S. Yoon, S.H. Hong, K. Kang and M. Kim, *Nano Energy*, 19 (2016) 234.
78. J. Lei, W. Li, X. Li and E.J. Cairns, *J. Mater. Chem.*, 22 (2012) 22022.
79. B. Liu, M. Cao, X. Zhao, Y. Tian and C. Hu, *J. Power Sources*, 243 (2013) 54.